Superconductivity and structure in sputtered Nb-Ta multilayers

P. R. Broussard
Naval Research Laboratory, Washington, D.C. 20375-5000

T. H. Geballe*
Department of Applied Physics, Stanford University, Stanford, California 94305
(Received 18 May 1987; revised manuscript received 7 August 1987)

The structure and superconducting properties of sputtered Nb-Ta multilayers are studied as a function of the bilayer period Λ. The films are mosaic structures with single-crystal diffraction profiles. The elastic mean free paths in both the niobium and tantalum layers are larger than the layer thicknesses. The measured transition temperatures and perpendicular critical field slopes are compared to the predictions of proximity theory. The parallel critical fields and angular dependences are examined for the occurrence of a three-dimensional to two-dimensional crossover.

INTRODUCTION

The study of the upper critical magnetic field H_{c2} in metallic multilayers is still a very promising field, as shown in the recent work on Mo-V.[1] In this paper, we extend the measurements on Nb-Ta multilayers given in our earlier work.[2] Here we examine the dependence of the critical temperature and upper critical field for both perpendicular and parallel orientations as a function of the bilayer period, Λ.

PREPARATION AND ROUTINE CHARACTERIZATION

Preparation of the multilayers is described in Ref. 2 with differences noted here. The samples were deposited at 750 °C onto $(1\bar{1}02)$ and $(11\bar{2}0)$ orientations of sapphire, with the bilayer period, Λ, varying from 3.4 Å (alloy sample) to 452 Å. X-ray measurements were made on both orientations, with critical-field measurements made only on the $(1\bar{1}02)$ samples. The ratio of the niobium to tantalum layer thickness is 1.3 with tantalum forming the top and bottom layers. The routine characterization is the same as in Ref. 2.

The layered nature of the samples is shown in Figs. 1 and 2, which show diffractometer scans along the growth direction for $\Lambda = 19.5$, 33.0, 54.4, and 94.1 Å on $(11\bar{2}0)$ sapphire. The low-angle reflections are shown in Fig. 1 and the satellites around the (110) reflection are shown in Fig. 2. Analysis of the x-ray intensities of the satellites (after accounting for Lorentz-polarization, absorption, and Debye-Waller effects) using the model of Kwo *et al.*[3] gives an interfacial width (defined as the distance where the tantalum concentration changes from 10% to 90%) of 6–7 Å for these samples.

The sample growth is identical to that in Ref. 2, with epitaxial registry to the sapphire and a single-crystal-like diffraction profile, verified by examining the in-plane order of the samples. For example, Fig. 3 shows a ϕ scan taken on the $\Lambda = 158$ Å sample on a $(11\bar{2}0)$ sapphire. This sample has the (110) reflection for Nb(Ta) parallel to the sample normal, and if it is a single crystal, by symmetry there will be two (200) reflections 45° away from the normal and 180° apart in ϕ. In Fig. 3, the Bragg-scattering condition is set for the (200) reflection of Nb(Ta), η is set to 45°, and then ϕ is scanned. We see two clear reflections 180° apart with no evidence for any other reflections. The difference in intensities is due to changes in the illuminated sample area. The inset in Fig. 3 shows the details of the scattering geometry. The full width at half maximum (FWHM) is approximately 1° of ϕ, whereas the instrumental resolution is $\approx 0.5°$. Therefore, if the sample is not a true single crystal, then the existing grains have only low-angle grain boundaries. Rocking-curve widths for the sample reflections are between 0.3 and 0.9°, with little difference for peaks both along and off the growth direction.

In Fig. 4 we show the low-temperature electrical resistivity (ρ_0) and the residual resistivity ratio (RRR) measured between room temperature and at 10 K. The saturation of ρ_0 for small values of Λ indicates the effect of the interfacial alloy becoming predominant. However, even in this limit, the elastic electron mean free path (the mean free path at low temperatures) is still longer than the bilayer period. As in Ref. 2, and from other works, we use for the ρl product (where ρ is the electrical resistivity in $\mu\Omega$ cm and l is the electron mean free path in Å) a value of 375 $\mu\Omega$ cm Å for both niobium and tantalum. The ρl product is dependent on the Fermi-surface area, and so will be essentially the same for Nb, Ta, and Nb-Ta alloys which are isoelectronic and have nearly identical crystal structures. Consider the simple model that the mean free path at low temperatures, l_0, is equal to the bilayer period, so that the resistivity of each layer will be $375/\Lambda$ in $\mu\Omega$ cm. By a parallel resistor model, the resistivity of the multilayer will then be

$$\frac{\Lambda}{\rho_0} = \frac{\Lambda}{\rho l}(d_{\mathrm{Nb}} + d_{\mathrm{Ta}}) \text{ or } \rho_0 = \frac{\rho l}{\Lambda} \ . \tag{1}$$

The line in Fig. 4 shows the result of this model. Clearly this overestimates the data, especially at small values of Λ.

We can apply the model of Gurvitch[4] to extract the individual layer resistivities, and then using our value of the ρl products, the layer mean free paths. There are several problems with this approach.

(a) Mean free paths larger than the layer thickness may invalidate the assumption of parallel resistors.

(b) We have not taken into account the variation of ρl with ρ_0, but since $\rho_0 < 10\ \mu\Omega$ cm, this is unlikely to be a problem.

(c) We have not taken the interface into account, so for small Λ the values of the mean free path may be meaningless.

Nonetheless, this approach still gives us some useful results. The results for the low-temperature mean free paths in each layer are shown in Fig. 5. We see that under these assumptions, the mean free path is larger than the layer thickness, and that the mean free path is much larger in niobium than tantalum. We have noted earlier[2] that our pure tantalum films have a smaller mean free path than for niobium films under the same deposition conditions, so this is consistent, if not yet explained.

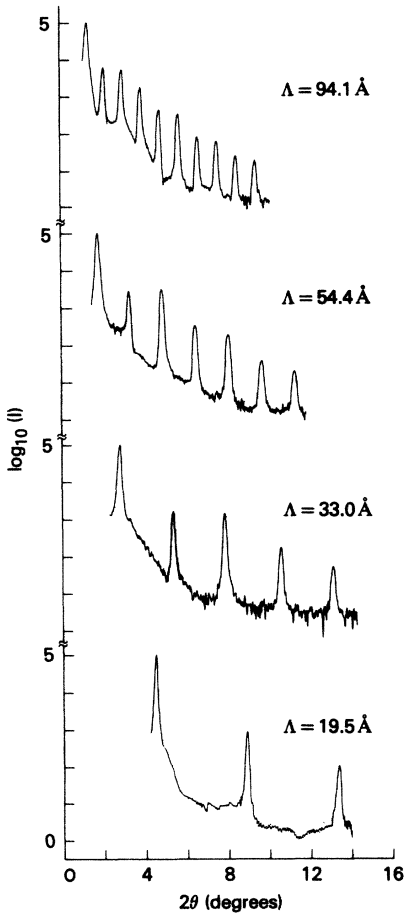

FIG. 1. X-ray scans along the growth direction for different bilayer periods grown on $(11\bar{2}0)$ sapphire showing the low-angle satellites.

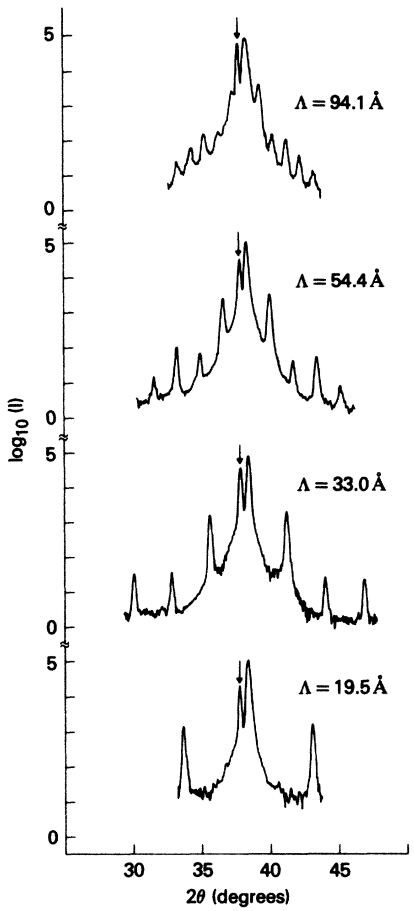

FIG. 2. X-ray scans along the growth direction for the samples in Fig. 1 near the (110) reflection for Nb and Ta. Arrows indicate the reflection due to the substrate.

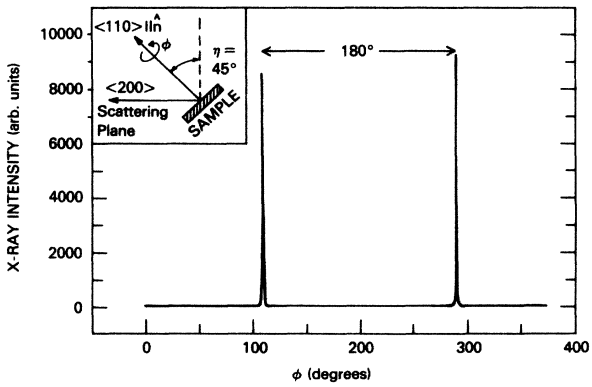

FIG. 3. X-ray intensity vs ϕ, the angle of rotation about the sample normal, for the $\Lambda = 158$ Å sample on $(11\bar{2}0)$ sapphire. The inset shows the scattering geometry. The sample normal is 45° away from the scattering plane, and the Bragg condition is set for the (200) reflection of Nb and Ta.

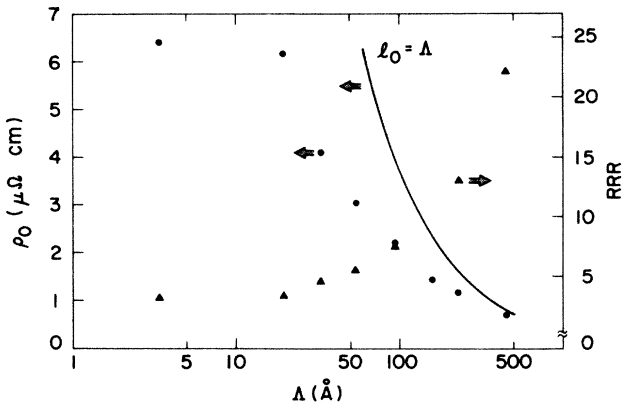

FIG. 4. The low-temperature resistivity ρ_0 (circles) and RRR (triangles) vs Λ for samples on $(1\bar{1}02)$ sapphire. The line is the calculated resistivity for a mean free path equal to the bilayer period.

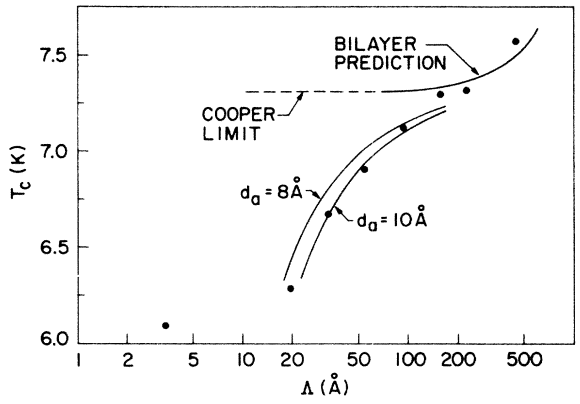

FIG. 6. T_c vs Λ for the samples on $(1\bar{1}02)$ sapphire (circles). The curves marked $d_a = 8$ and 10 Å are trilayer fits [Eq. (5)] with the interfacial alloy thickness set to 8 and 10 Å, respectively. The bilayer prediction uses the mean free path of Fig. 5, and Eqs. (2)–(4).

SUPERCONDUCTING CRITICAL TEMPERATURE

T_c was measured by a resistive technique, and the results are shown in Fig. 6. The decrease in T_c at small Λ is indicative of the formation of an interfacial alloy, which has a lower T_c than the niobium layers. We can examine the data in light of proximity-effect theory, if we remember that the theories for bilayer systems have typically dealt with metals in the dirty limit, defined by $\lambda_{\text{transport}} \gg 1$, where $\lambda_{\text{transport}}$ is given by

$$\lambda_{\text{transport}} = 0.882\xi_0/l_0 \ .$$

Here ξ_0 is the Bardeen-Cooper-Schrieffer (BCS) coherence length, and l_0 is the elastic mean free path. From the calculated mean free paths above, the $\Lambda = 452$ Å sample will have $\lambda_{\text{transport}}(\text{Nb}) \approx 0.4$ and $\lambda_{\text{transport}}(\text{Ta}) \approx 6$, so while the dirty-limit approximation may be valid for the tantalum layers, it will not be in the niobium layers.

For samples with large Λ, we start with the de Gennes–Werthamer[5,6] proximity-effect equations. Since our samples are not in the dirty limit, a more exact expression for the equation relating the relevant length scales in each material to the temperature is needed. We use the approach as in Kogan's work,[7] which gives for the exact expression,

$$\frac{\hbar}{2\pi k_B T}\ln\left[\frac{T_c}{T}\right] = \sum_{\omega>0}\left[\frac{1}{\omega} - 2\tau\frac{f(k_{S,N}l_0/\beta)}{k_{S,N}l_0 - f(k_{S,N}l_0/\beta)}\right]$$

$$\text{where } f(x) = \begin{cases} \arctan(x) & \text{for } T < T_c \ , \\ \operatorname{arctanh}(x) & \text{for } T > T_c \ , \end{cases} \qquad (2)$$

$k_{S,N}$ is the inverse length scale for each material, $\beta = 1 + 2\omega\tau$, $\hbar\omega = \pi k_B T(2n+1)$ $(n = 0,1,2,\ldots)$, $\tau = l_0/v_F$, T_c is the transition temperature, and v_F is the Fermi velocity for each material. In the dirty limit, this reduces to the diffusion equation of de Gennes–Werthamer. We use the bulk transition temperatures for each material, and for the Fermi velocity of niobium, we use the calculated value found by Kerchner *et al.*,[8] $\langle v_F^2 \rangle^{1/2} = 2.7 \times 10^7$ cm/s. For tantalum, we use the equations listed by Orlando *et al.*[9] and again assume that the Fermi surfaces of niobium and tantalum are similar, which gives $\langle v_F^2 \rangle^{1/2} = 3.6 \times 10^7$ cm/s.

The choice of boundary conditions, of course, is much more difficult. We have chosen to use the standard de Gennes–Werthamer boundary conditions, although they have been derived under certain assumptions. We have modified them, however, since they call for the use of a dirty-limit value of the coherence length ξ,

$$\xi = \left[\frac{\hbar v_F l_0}{6\pi k_B T}\right]^{1/2}$$

and as mentioned, this will not be correct for our samples. Silvert[10] has studied the proximity-effect question and boundary conditions. He found that the more exact formulation followed a scaling as in the dirty limit, if one replaced the above coherence length with

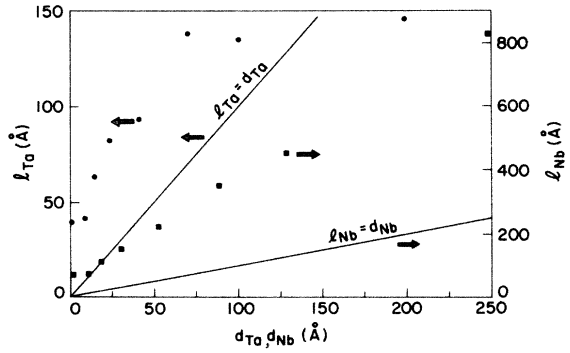

FIG. 5. Calculated elastic mean free paths in the tantalum layers (circles) and niobium layers (squares) vs the layer thickness. The lines are where the mean free path is equal to the layer thickness. Notice that most of the points fall above their respective lines.

$$\frac{1}{\xi^2}=\frac{t}{\Xi_0}\left[\frac{3}{\Xi_0}+\frac{3}{l_0}\right],\quad \Xi_0=\frac{\hbar v_F}{2\pi k_B T_c},\quad t=T/T_c\ . \tag{3}$$

Obviously as $l_0\to 0$, or $\lambda_{\text{transport}}$ becomes much larger than 1, this definition approaches the dirty-limit value. For multilayers the fully periodic boundary condition is typically used, where one can map an infinite multilayer with layer thicknesses of d_S and d_N onto a bilayer with $\frac{1}{2}$ the original layer thicknesses. However, preliminary experiments and calculations[11] and work done by Arnold at Notre Dame[12] indicate that for a finite multilayer the proximity-effect T_c is not dependent on the number of periods. Therefore, we use the standard bilayer equation,

$$k_S\tan k_S d_S=\eta k_N\tanh k_N d_N\ , \tag{4}$$

where $d_S+d_N=\Lambda$, and

$$\eta=(\gamma\xi^2)_{\text{normal}}/(\gamma\xi^2)_{\text{superconducting}}\ .$$

We use published values for the electronic coefficient of specific heat γ (7195 ergs/cm^{3}K^2 for niobium, and 5413 ergs/cm^{3}K^2 for tantalum) and the values of the elastic mean free path obtained in the earlier section. The results of this calculation are shown in Fig. 6 as the curve labeled bilayer prediction. Notice that the curve tends to underestimate the T_c for the largest value of Λ, and that the use of the infinite-multilayer model would have made this even worse.

In the region of $\Lambda<200$ Å, we must obviously include the effect of the alloy interface. We can use an extension of the Cooper limit in the same way as Lowe[13] did for Nb-Zr multilayers, if the relevant sample dimensions are less than a coherence length. The critical-field data for $\Lambda=158$ Å give a value for $\xi_{\text{GL}}(0)\approx 153$ Å (GL denotes Ginzburg-Landau), so this condition is satisfied. Silvert[14] has pointed out that for the case of strong coupling, the Moorman sum rules[15] for the Cooper limit will give for the T_c of the system,

$$\ln T_c=\frac{\langle\lambda\ln\Theta_D\rangle}{\langle\lambda\rangle}-\frac{1}{\lambda^*}-\ln 1.45\ , \tag{5}$$

where the averages are evaluated as

$$\langle A\rangle=\frac{\sum_{\text{layers}} A_i N_i d_i}{\sum_{\text{layers}} N_i d_i}\ , \tag{6}$$

with N_i and d_i being the density of states and layer thickness of layer i, respectively. Here λ is the electron-phonon mass enhancement for each material, as found using McMillan's[16] equation,

$$T_c=\frac{\Theta_D}{1.45}\exp(-1/\lambda^*),\quad \lambda^*=\frac{\lambda-\mu^*-0.62\mu^*\lambda}{1.04(1+\lambda)}\ , \tag{7}$$

where μ^* is the Coulomb repulsion term, set to the canonical value 0.13 for transition metals, and Θ_D is the Debye temperature for each material. In Eq. (5), λ^* is defined by replacing λ in Eq. (7) by $\langle\lambda\rangle$. We represent the interface as a layer of 50 at.%–50 at.% alloy of thickness d_a with a T_c of 5.9 K. The reason for this choice is that although the entire film has a global average of some composition, at the interface the local average will be that of an equal-composition alloy. The parameters used in this case are listed in Table I, and the fits to the small-Λ data are shown in Fig. 6, showing the reduction in T_c due to the proportional increase of the interfacial alloy. In the two fits the interface width is chosen to be 8 and 10 Å. The results from the x-ray analysis earlier indicated that the interface width would be $\lesssim 7$ Å, but the T_c data below $\Lambda=100$ Å fit best to a 10-Å interface width. This discrepancy may be due to the use of a discrete layer system, when the actual multilayer has a smooth variation in composition. The use of a more realistic composition profile, along with accurate values for Θ_D, λ, and N as a function of concentration may give better agreement with the x-ray results for the interfacial width.

TABLE I. Trilayer fit parameters.

	Nb	Ta	$Nb_{0.5}Ta_{0.5}$
Θ_D (K)	277	258	266
N (states/eV atom spin)	1.65	1.27	1.40
λ	0.821	0.644	0.702
T_c (K)	9.2	4.4	5.9

UPPER CRITICAL FIELD

The upper critical field, H_{c2}, was measured in the same manner as in Ref. 2. We first turn to the results for the perpendicular critical-field measurements. Figure 7 shows the measured critical-field slopes versus Λ. At small Λ, we see a saturation close to that measured in bulk Nb-Ta alloys.[17] As Λ increases, there is a rapid drop in the slope, which we will discuss later. For com-

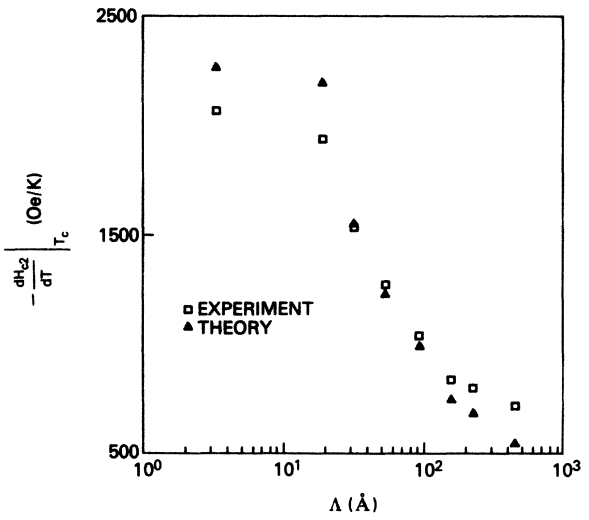

FIG. 7. Measured perpendicular critical-field slopes (squares) and calculated values (triangles) from Eqs. (2), (3), and (8) vs Λ.

parison, a pure niobium film made under similar conditions[2] has a T_c of 9.22 K, a RRR of 160, and an upper-critical-field slope of 510 Oe/K.

In Fig. 8 we examine the trend of the positive curvature in our samples. Figure 8(a) shows the value of the reduced field at a reduced temperature of 0.4 as a function of bilayer period, Λ. We see a clear increase up to Λ of 94.1 Å, a local maximum, and then another increase at Λ of 452 Å. Figure 8(b) looks at the deviation-function plots (as in Ref. 8) for $\Lambda=33.0$, 94.1, and 452 Å. For $\Lambda \leq 33$ Å, the curves are identical to the clean-limit curve of Hefland and Werthamer.[18] Notice that the behavior of the $\Lambda=94.1$ Å curve differs at low t from the $\Lambda=452$ Å curve. The importance of this difference will be discussed later.

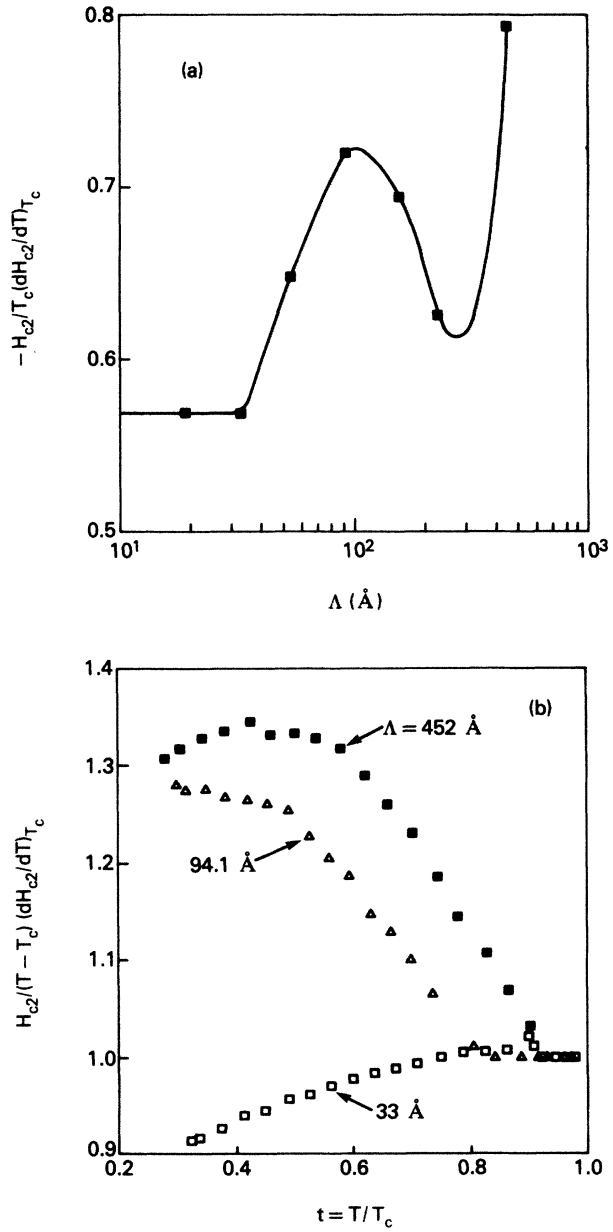

FIG. 8. (a) Reduced perpendicular upper critical field vs Λ at a reduced temperature of 0.4. A value greater than 0.6 indicates positive curvature. The line is a guide to the eye. (b) Deviation plots for $\Lambda=33.0$, 94.1, and 452 Å.

We can examine both the trend in the critical-field slope and the positive curvature using the theory of Biagi, Kogan, and Clemm[19] with some modifications. The results of this theory are basically those of the proximity-effect theory using a modification of the boundary condition, Eq. (4) to

$$q_S \tan q_S d_S = \eta q_N \tanh q_N d_N \ , \qquad q_{S,N}^2 = k_{S,N}^2 \mp \frac{2\pi H_{c2}}{\phi_0} \ . \tag{8}$$

As we have pointed out in Ref. 2, their theory is a dirty-limit calculation, and the neglect of the magnetic field dependence of k means that the temperature dependence cannot be fully obtained.[7] However, we can approach this in another way. Near the T_c of the multilayer, the magnetic field dependence of $k_{S,N}$ is not important,[7] so we can neglect it for obtaining the critical-field slope of the multilayer. To eliminate the dirty-limit approximation, we use the exact expression for $k_{S,N}(T)$, Eq. (2), and use the elastic mean free paths found earlier. In the work of Biagi *et al.*, they allowed η to vary. As in the T_c calculation, we have fixed it at the value for the de Gennes–Werthamer boundary condition. Obviously this approach gives for the T_c the value calculated for a bilayer as in Fig. 6. The values of the calculated slope, shown in Fig. 7, however, agree remarkably well with the experimental data. Therefore, although the theory cannot describe the behavior of T_c without including an interface contribution, it can predict the behavior of the critical-field slope, and indicates that the reduction in mean free path is the major factor.

The behavior of the positive curvature seen in these samples cannot, however, be explained by the model of Biagi *et al.* Calculations of the positive curvature in the reduced field as a function of Λ for our parameters show a monotonic trend, decreasing as Λ increases and always negative. In our case, however, we see a maximum in the positive curvature near $\Lambda=94.1$ Å, and then another increase at $\Lambda=452$ Å. The second increase we attribute to Fermi-surface anisotropy as seen in Ref. 8. There is a strong similarity between the shape of the deviation-function plots for the $\Lambda=452$ Å sample and those for niobium in Ref. 8. As noted earlier, there is a difference in the shape of the deviation plot between the $\Lambda=94.1$ Å sample and the $\Lambda=452$ Å sample, implying that the positive curvature here is not due primarily to Fermi-surface effects. The maximum at $\Lambda=94.1$ Å in the positive curvature is as yet unexplained, but we believe that the proximity effect is the cause.

PARALLEL CRITICAL FIELD AND ANGULAR DEPENDENCE

For samples in the strongly coupled regime, the temperature dependence of the parallel upper critical field should be similar to that for the perpendicular, and the angular dependence will be three-dimensional- (3D) like, obeying[20]

$$H_{c2}(T,\theta)=\frac{H_{c2\perp}(T)}{[(m/M)\sin^2\theta+\cos^2\theta]^{1/2}}\ ,$$
$$\frac{M}{m}=\left[\frac{H_{c2\parallel}(T)}{H_{c2\perp}(T)}\right]^2\ , \tag{9}$$

where θ is the angle between the field direction and the sample normal. For samples with $\Lambda \leq 250$ Å, we find that although the temperature dependence of the parallel critical field indicates that the samples are in the 3D regime, the angular dependence shows a trend from 2D behavior for small Λ to 3D behavior at larger Λ, as shown in Fig. 9. The angular dependence for the 2D case is given implicitly by[21]

$$\left[\frac{H_{c2}(T,\theta)\cos\theta}{H_{c2\perp}(T)}\right]+\left[\frac{H_{c2}(T,\theta)\sin\theta}{H_{c2\parallel}(T)}\right]^2=1\ . \tag{10}$$

Notice that as Λ increases, the behavior at $\theta=90°$ for our samples goes from cusplike to a plateau, indicative of 3D behavior. Behavior similar to this has been seen by Ruggiero[22] and Banerjee,[23] and surface-state superconductivity has been proposed as an explanation, although it is not clear that this a satisfactory answer. For our films, the initial and final layers are tantalum, so one expects surface-state superconductivity to be suppressed.

At $\Lambda=452$ Å, we see a change in the behavior of the parallel critical field. Figure 10 shows the ratio of parallel to perpendicular critical field versus Λ at a reduced temperature of 0.6. The jump at $\Lambda=452$ Å is similar to that seem in Nb-Cu (Ref. 23) and prediced to occur in proximity systems by Takahashi and Tachiki[24] in the case of 3D-to-2D crossover. We can also see the change in behavior by looking at the critical fields for the $\Lambda=452$ Å sample, as in Fig. 11(a). While the temperature dependence of $H_{c2\perp}$ shows no evidence for negative curvature, in $H_{c2\parallel}$ there is negative curvature as well as a kink at $T\approx 6$ K. If this is a signature of 3D-to-2D crossover, we would expect that the angular dependence of the critical field below the transition would follow a 2D behavior. What we find for this sample, as shown in Fig. 12, is more complicated. For $\theta < 50°$, the data follow a 3D curve, while above this the data fall below and at $\theta=90°$ there is a cusp. We point out that it may be plausible for the vortex structure in a multilayer sample to behave as 3D for fields near perpendicular, and to spontaneously change as the field approaches parallel. The current theories of the proximity effect have not as yet calculated the angular dependencies for samples in the crossover region.

Although the 2D nature of the sample is not conclusively shown, we can obtain some insight into this behavior by examining the data in a simple manner. According to Tinkham,[21] the upper critical field for a 2D film will be given by

$$H_{c2\parallel}(T)=\frac{\sqrt{12}\phi_0}{2\pi\xi_\parallel(T)d_S}=\frac{\sqrt{12}\phi_0}{2\pi\xi_\parallel(0)d_S}(1-T/T_c)^{1/2}\ ,$$

where the last equality will hold in the GL limit. (Kogan[25] has shown that the above equation is valid only in the dirty limit, and for cleaner samples must be modified. For our simple approach, we will use the

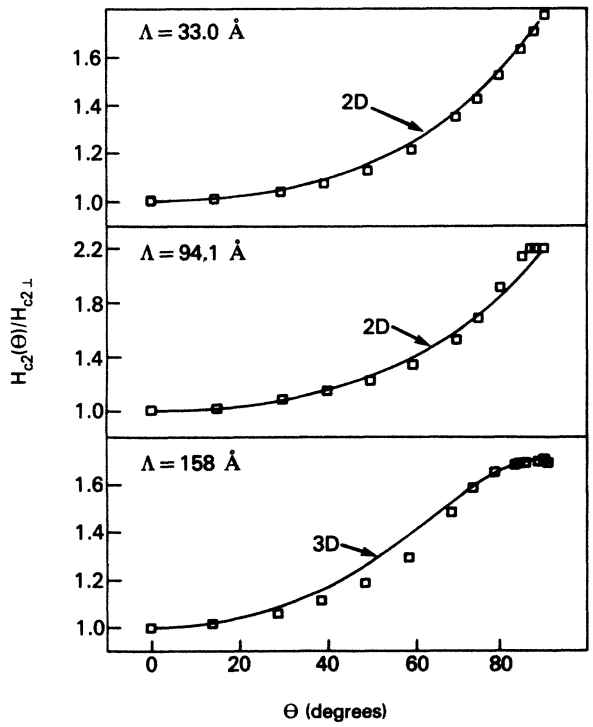

FIG. 9. Angular dependence of the upper critical field at a reduced temperature of 0.9 for $\Lambda=33.0$, 94.1, and 158 Å. Curves marked 2D are fitted to Eq. (10), and 3D to Eq. (9).

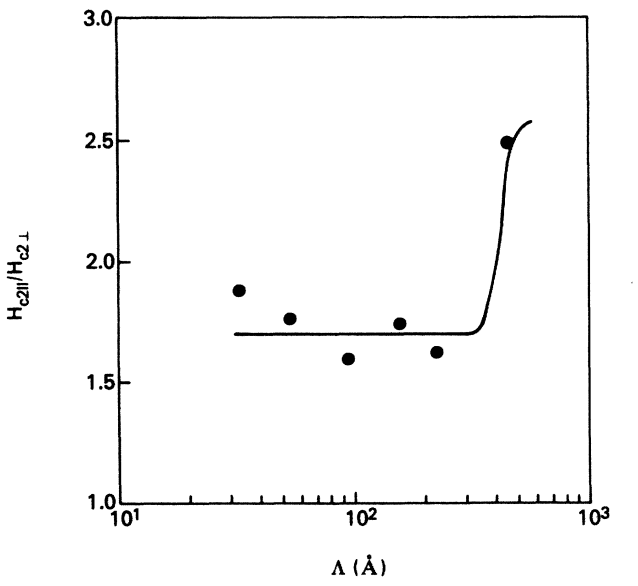

FIG. 10. Ratio of parallel to perpendicular critical field vs Λ at a reduced temperature of 0.6. Dimensional crossover is indicated by an enhancement of this ratio. The line is a guide to the eye.

above equation.) Here d_S and T_c are the thickness and transition temperature for the thin film. In our case, the occurrence of 2D behavior occurs far below the T_c of the sample and so the GL requirement may not be met. However, for *SN* proximity systems,[24] calculations have shown that $(H_{c2\|})^2 \propto T$ behavior can exist far below T_c. What we can attempt to do is to fit the data in the 2D regime to a modified 2D equation,

$$H_{c2\|}^2(T)=\left[\frac{\sqrt{12}\phi_0}{2\pi\xi_{\|}(0)d_{\text{eff}}}\right]^2\left[1-\frac{T}{T^*}\right], \tag{11}$$

where d_{eff} and T^* are the effective thickness and 2D transition temperature for the thin niobium layers. The resulting fit for $\Lambda=452$ Å is shown in Fig. 11(b). The fit

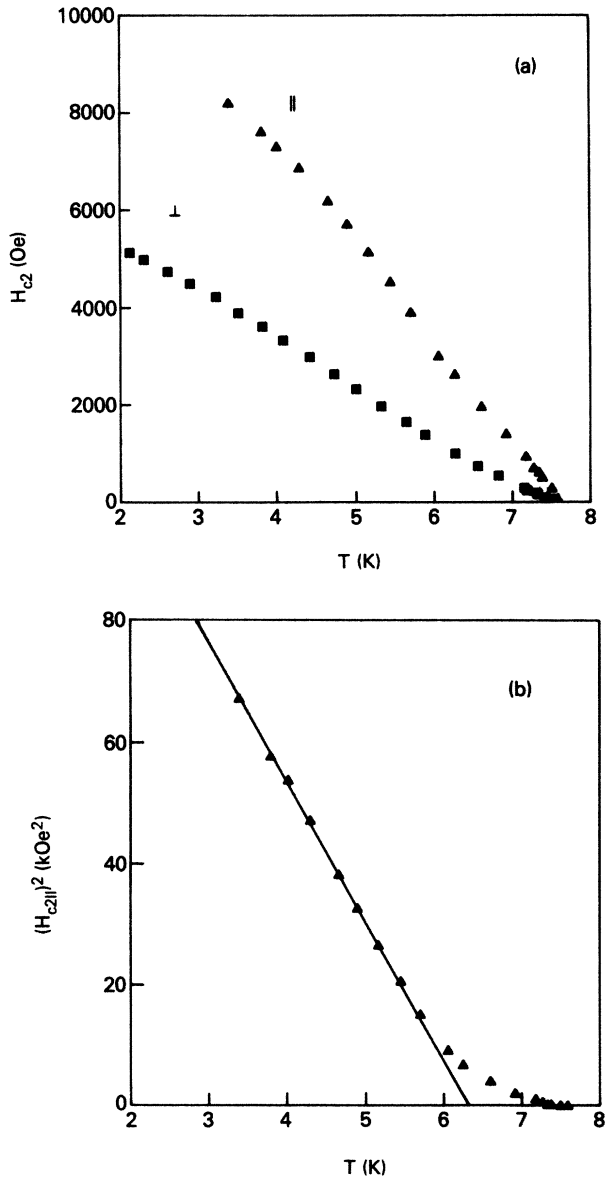

FIG. 11. (a) Temperature dependence of the parallel and perpendicular critical field for the $\Lambda=452$ Å sample. (b) Plot of $(H_{c2\|})^2$ vs T for the data in the 2D region.

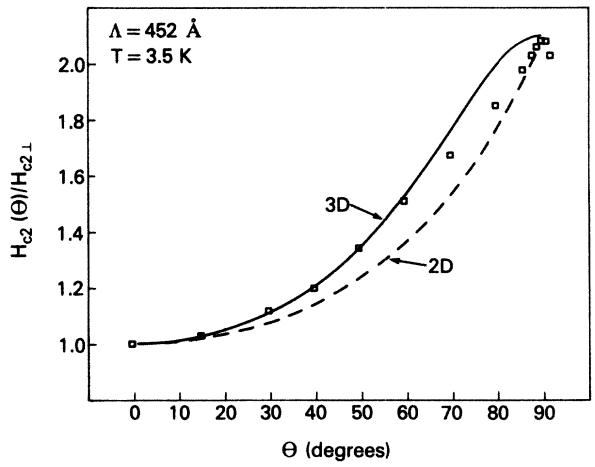

FIG. 12. Angular dependence of the upper critical field for $\Lambda=452$ Å. The curves are fits to the 3D and 2D equations.

parameters are $d_{\text{eff}}=400$ Å and $T^*=6.3$ K. A similar analysis can be performed on the data of Sample 9 in Ref. 2, with the result of $d_{\text{eff}}=260$ Å and $T^*=3.1$ K. From the known niobium layer thicknesses, we obtain excess thicknesses (d_+) of 144 and 162 Å for these samples. If we assume that the excess thickness is due to the order parameter "leaking" into the tantalum layers, we see that the penetration into each tantalum layer is about 70–80 Å. In addition, if we use the standard definition of the perpendicular coherence length,

$$\xi_{\perp}(T)=\left[\frac{\phi_0 H_{c2\perp}}{2\pi H_{c2\|}^2}\right]^{1/2},$$

we find that we obtain values for $\xi_{\perp}(T^*)/\Lambda$ of 0.51 and 0.43 for these samples. From Josephson-coupling theories of multilayers,[26] the 3D-to-2D crossover point is given by $\xi_{\perp}(T^*)/\Lambda=1/\sqrt{2}$. Our values seem to point to a different relation, such as $\xi_{\perp}(T^*)/\Lambda=\frac{1}{2}$. We point out that results on V-Ag multilayers[27] indicate that the crossover occurs at

$$\xi_{\perp}(T^*)/\Lambda=[(\pi\sqrt{3})^{1/2}]^{-1}\approx 0.43$$

or when the vortex periodicity matches the multilayer period. The above agrees reasonably well with our results. Kanoda *et al.* also noticed another transition at $\xi_{\perp}(T^*)/2\Lambda\approx 0.43$ which they interpreted as due to a doubly commensurate structure between the vortex lattice and the multilayer. As of yet, we have not observed such a transition in our samples.

CONCLUSIONS

We have shown that our Nb-Ta multilayers have a mosaic structure with a single-crystal diffraction profile. The electrical resistivity at small Λ is limited by scattering due to Nb-Ta alloy at the interfaces, while at large Λ resistivity drops rapidly. Analysis of the resistivity shows that the longitudinal mean free path (at low temperatures) for each layer is longer than the layer thick-

ness, with the niobium mean free path substantially longer than that for tantalum. The effect of the interface is very strong in determining the transition temperature for the small-Λ limit, while the critical-field slope is more dependent on the mean free path. The theory of Bragi, Kogan, and Clemm cannot explain the positive curvature observed for the perpendicular critical field, which we feel is due to the proximity effect for small Λ and Fermi-surface effects for large Λ. The parallel critical field for Λ below 450 Å shows 3D temperature dependence, but the angular dependence goes from 2D-like to 3D as Λ increases. For $\Lambda=452$ Å, we observe a transition in the parallel critical field which we interpret as a 3D-to-2D crossover. The angular dependence is 3D-like near perpendicular, but goes over to 2D near parallel. Analysis of the parallel critical field agrees with an earlier[27] definition of 3D-to-2D crossover, and the effective superconducting thickness is given by the niobium layer thickness plus an amount due to penetration of the order parameter into the tantalum layers.

ACKNOWLEDGMENTS

We would like to acknowledge many helpful discussions with G. Arnold and V. Kogan. This work was supported principally by the U.S. Air Force Office of Scientific Research under Contract No. F49620-83-C-0014. Samples were prepared at the Stanford University Center for Materials Research, supported by the National Science Foundation Materials Research Laboratories Program. Part of this work was done while one of us (P.R.B.) was supported by the National Research Council.

*Also at Bell Communications Research, Red Bank, NJ 07701-7020.

[1]M. G. Karkut, D. Ariosa, J.-M. Triscone, and Ø. Fischer, Phys. Rev. B **32**, 4800 (1985).
[2]P. R. Broussard and T. H. Geballe, Phys. Rev. B **35**, 1664 (1987).
[3]J. Kwo, M. Gyorgy, D. B. McWhan, M. Hong, F. DiSalvo, C. Vettier, and J. E. Bower, Phys. Rev. Lett. **55**, 1402 (1985).
[4]M. Gurvitch, Phys. Rev. B **34**, 540 (1986).
[5]P. G. De Gennes, Rev. Mod. Phys. **36**, 225 (1964).
[6]N. R. Werthamer, Phys. Rev. **132**, 2440 (1963).
[7]V. Kogan, Phys. Rev. B **32**, 139 (1985).
[8]H. R. Kerchner, D. K. Christen, and S. T. Sekula, Phys. Rev. B **24**, 1200 (1981).
[9]T. P. Orlando, E. J. McNiff, Jr., S. Foner, and M. R. Beasley, Phys. Rev. B **19**, 4545 (1979).
[10]William Silvert, J. Low Temp. Phys. **20**, 439 (1975).
[11]P. R. Broussard, Ph.D. dissertation, Stanford University, 1986.
[12]G. Arnold (private communication).
[13]W. P. Lowe and T. H. Geballe, Phys. Rev. B **29**, 4961 (1984).
[14]W. L. Silvert, Phys. Rev. B **12**, 4870 (1975).
[15]W. Moorman, Z. Phys. **197**, 136 (1966).
[16]W. L. McMillan, Phys. Rev. **167**, 331 (1968).
[17]T. Ogasawara, Y. Kubota, and K. Yasukochi, Phys. Lett. **24A**, 463 (1967).
[18]E. Hefland and N. R. Werthamer, Phys. Rev. **147**, 288 (1966).
[19]K. R. Biagi, V. G. Kogan, and J. R. Clemm, Phys. Rev. B **32**, 7165 (1985).
[20]W. Lawrence and S. Doniach, in *Proceedings of the 12th International Conference on Low Temperature Physics, Kyoto, Japan, 1970,* edited by E. Kanada (Keigaku, Tokyo, 1971), p. 361.
[21]M. Tinkham, Phys. Rev. **129**, 2413 (1963).
[22]S. T. Ruggiero, T. W. Barbee, Jr., and M. R. Beasley, Phys. Rev. B **26**, 4894 (1982).
[23]I. Banerjee and I. K. Schuller, J. Low Temp. Phys. **54**, 501 (1984).
[24]S. Takahashi and M. Tachiki, Phys. Rev. B **33**, 4620 (1986).
[25]V. G. Kogan, Phys. Rev. B **34**, 3499 (1986).
[26]R. A. Klemm, M. R. Beasley, and A. Luther, J. Low Temp. Phys. **16**, 607 (1974).
[27]K. Kanoda, H. Mazuki, T. Yamada, N. Hosoito, and T. Shinjo, Phys. Rev. B **33**, 2052 (1986).